J Mol Model (2013) 19:3719–3731
DOI 10.1007/s00894-013-1906-9

ORIGINAL PAPER

The effect of cross linking density on the mechanical properties and structure of the epoxy polymers: molecular dynamics simulation

Ali Shokuhfar · Behrouz Arab

Received: 6 May 2013 / Accepted: 30 May 2013 / Published online: 22 June 2013

Abstract Recently, great attention has been focused on using epoxy polymers in different fields such as aerospace, automotive, biotechnology, and electronics, owing to their superior properties. In this study, the classical molecular dynamics (MD) was used to simulate the cross linking of *diglycidyl ether of bisphenol-A (DGEBA)* with *diethylenetriamine (DETA)* curing agent, and to study the behavior of resulted epoxy polymer with different conversion rates. The constant-strain (static) approach was then applied to calculate the mechanical properties (Bulk, shear and Young's moduli, elastic stiffness constants, and Poisson's ratio) of the uncured and cross-linked systems. Estimated material properties were found to be in good agreement with experimental observations. Moreover, the dependency of mechanical properties on the cross linking density was investigated and revealed improvements in the mechanical properties with increasing the cross linking density. The radial distribution function (RDF) was also used to study the evolution of local structures of the simulated systems as a function of cross linking density.

Keywords Cross linking · Epoxy polymer · Mechanical properties · Molecular dynamics · Radial distribution function

Introduction

Epoxies are thermosetting polymers with linear or 3D cross-linked structures, typically obtained from reaction between epoxy resins and proper curing agents (hardeners). The main parameters controlling the polymer structure are the functionality of monomers, the molar ratio between initiator and monomers, the concentration of species that are involved in chain transfer steps, and temperature (thermal cycle) that affects the relative rates of different steps [1]. Among them, the functionality of reactants, i.e. the number of reactive sites per monomer, determines whether the final structure of yielded polymer would be linear or cross-linked. There are three types of reactants, regarding their functionality: mono-functional, bi-functional, and multi-functional. The bi- and multi-functional reactants lead to formation of linear and cross-linked structures respectively, while the mono-functional ones produce short discrete chains, and hence would return relatively weak material properties. To achieve 3D cross-linked structures, at least one of reactants (resin or hardener) must be multifunctional.

The cross links are irreversible covalent bonds and the cross-linked polymers cannot be re-melted and re-shaped. Epoxies with 3D cross-linked structures have superior properties, making them attractive materials for different applications including coatings, composite materials, adhesives, electronic packaging, etc.

Previously, investigation of the effects of different parameters on the final properties of cross-linked polymers was mainly based on experimental trial and error methods, while the big challenge in development of polymer-based materials is to understand the fundamental phenomena in different length and time scales. In recent years, however, considerable attention has been paid to using the predictive modeling and simulation approaches for development of polymers and polymer (nano)composites [2], especially nowadays that a wide range of well-optimized simulation methods in different length and time scales are available along with the powerful computational facilities.

A. Shokuhfar · B. Arab (✉)
Advanced Materials and Nanotechnology Research Lab,
Faculty of Mechanical Engineering, K. N. Toosi University
of Technology, P.O. Box: 19395-1999, Tehran, Iran
e-mail: arab@dena.kntu.ac.ir

Among different research aspects related to polymers, few attempts have been made to study the dynamics of cross linking process and structure–property relationship of cross-linked polymers and their composites. For instance, Doherty et al. [3] developed a polymerization molecular dynamics (MD) scheme to construct cross-linked poly(methacrylates) (PMA) networks. By means of large-scale MD simulations, Tsige and Stevens [4] investigated the effect of cross-linker functionality and interfacial bond density on the fracture behavior of highly cross-linked polymer networks. Komarove et al. [5] used mapping and reverse mapping of data, and combined coarse grained Monte Carlo (MC) and atomistic MD for creating and characterizing the cross-linked polymers. Employing the MD method, the cross linking of poly(vinyl alcohol) (PVA) with polyol curing agent was simulated by Bermegjo and Ugarte [6, 7], and the material properties of the cross-linked polymer were calculated. Hölck et al. [8] studied the thermo-mechanical behavior of the polymer obtained from cross linking between epoxy phenol novolac (EPN) and bisphenol-A hardener. They also investigated the bulk properties of the polymer, interfacial properties of the cross-linked EPN and SiO_2 layers, and the mobility of the water molecules in constructed polymer, by means of MD. Some researchers studied the epoxy polymers resulted from EPON 862 resin cross-linked with diethyltoluenediamine (DETDA) [9–13] and triethylenetetramine (TETA) [14–17] curing agents. Cross linking of DGEBA resin with isophorone diamine (IPD) [18–21], trimethylene glycol di-*p*-aminobenzoate (TMAB) [22], DETDA [23], diamine [24], diaminodiphenyl sulfone (DDS) [25], methylenedianiline (MDA) [26], and poly (oxypropylene) (POP) diamines [27] were simulated and studied by some others. There are also some studies based on MD simulations of behavior of cross-linked epoxy polymers reinforced with Al_2O_3 [15], SiC [16, 17] and poly (oligomeric silsesquioxane) (POSS) [22] nanoparticles, and carbon nanotubes (CNT) [28–30]. More research studies related to modeling and simulation of cross-linked polymers and their composites can be found in the literature [31–36].

The epoxy resin, diglycidyl ether of bisphenol-A (DGEBA) also known as EPON 828, can be cross-linked in presence of diethylenetriamine (DETA) curing agent to yield one of the frequently used epoxy polymers in structural composites and coatings. The DGEBA/DETA compound has been recently used to synthesize the epoxy matrix in self healing polymer composites [37–43], as a new generation of smart materials. The more detailed structures of DGEBA and DETA are given in the next section.

To authors' knowledge, there is no similar study on molecular simulation of epoxy EPON 828 cross-linked with DETA curing agent. Molecular dynamics, as one of the most effective and popular simulation methods, is used to study the structure and mechanical properties of the cross-linked epoxy polymers with different cross linking densities.

Modeling and simulation details

Software and force-field

All simulations were performed using Accelrys Materials Studio 5.5 software package [44]. The *condensed-phase optimized molecular potentials for atomistic simulation studies (COMPASS)* force-field was employed in all molecular mechanics and dynamics simulations. COMPASS, as the new version of *polymer consistent force-field (PCFF)*, is a class II force-field parameterized for different molecules including most common organics, small inorganic molecules, and polymers to predict various properties of the materials [45–50].

The total energy function in COMPASS force-field is composed of 12 terms including *valence* and *non-bonded interaction* terms [45]. Valence terms fall into two categories: *diagonal* (bond stretching, bending, torsion, and out-of-plane potentials), and *off-diagonal cross-coupling* terms (describing the interactions between diagonal terms). The non-bonded interactions, including relatively short range van der Waals (vdW) and long range electrostatic interactions, are described by Lennard-Jones (LJ) 9–6 and Coulombic functions, respectively.

In all simulations, the atom-based summation method with cut-off radii of 12.5 Å was used in calculation of the vdW interactions. Long range corrections was also applied on the cut-off radii to smoothly eliminate the non-bonded interactions over a range of distances and avoid the discontinuities caused by direct cut-offs. The electrostatic interactions, on the other hand, were dealt with through the Ewald summation method [51] with the accuracy of 10^{-4} kcal mol^{-1}.

Molecular structures of DGEBA and DETA before and after cross linking

The primary molecular structures of DGEBA resin ($C_{21}H_{24}O_4$) and DETA curing agent ($C_4H_{13}N_3$) are schematically represented in Fig. 1.

DGEBA is a bi-functional reactant with two *epoxide* groups at two ends, while DETA has five reactive sites including both

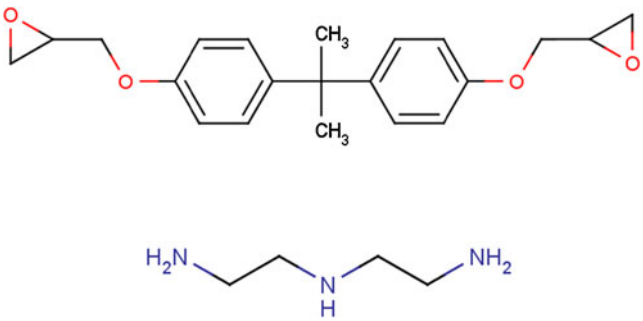

Fig. 1 Molecular structures of EPON 828 (top), and DETA (bottom), before cross linking

primary and secondary amine groups, and hence is a multi-functional (fivefold-functional) reactant. Therefore, DGEBA and DETA are able to produce 3D cross-linked epoxy polymers, as was mentioned earlier. Each DETA molecule can react at most with five DGEBA molecules, each of which are capable of being connected to another DETA molecule through its second epoxide head. Thus, the normal composition ratio of DGEBA/DETA in the blend is 5/2.

The $C-O$ bond in each epoxide group needs to be broken in order to form a reactive $-CH_2$ site (Fig. 2), capable of being cross-linked to DETA molecule.

In the blend of resin and hardener, under appropriate circumstances, the molecules start to move around and the curing sites will have the chance of getting sufficiently close to each other, so that the covalent bonds could be created between C and N atoms. A conversion rate of 100 % will be achieved if all potential covalent bonds are created, though it is rare in natural conditions. Figure 3 shows a fully cross-linked epoxy polymer, in which one DETA molecule is connected to five DGEBA molecules through covalent bonds.

Simulation of cross linking process

In order to obtain cross-linked epoxy polymers from resin and curing agent using MD method, there are two common ways: (i) Using a representative cross-linked molecule with a certain degree of cross linking, either created manually or extracted from a previously cross-linked structure [15, 16], then constructing the simulation box with given density and number of representative molecules, and finally, performing proper MD runs for equilibration and data collection. (ii) Creating a simulation box including primary molecules of resin and curing agent without any cross link, then performing a cyclic set of minimization, equilibration and dynamics runs to reach a satisfactory cross-linked structure, and finally, conducting further MD simulations for obtaining the properties of interest.

The second method is complicated and time consuming to establish, especially in the case of large systems. Nevertheless, it is more accurate and realistic than the first one, and hence is recommended to be used rather than the first method. Moreover, it can be applied flexibly with respect to many parameters such as, cross linking cut-off distance, content of curing agent, reaction priorities of the primary and secondary amines, etc.

Fig. 2 Conversion of a primary epoxide group to a reactive one through breaking the C−O bond

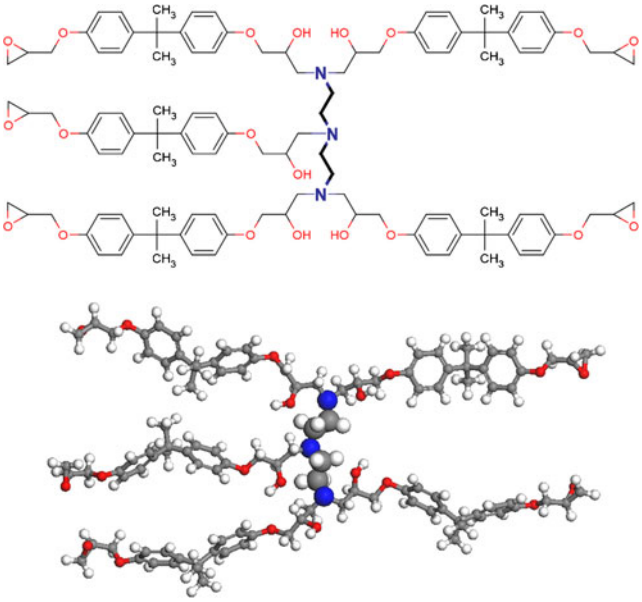

Fig. 3 Schematic 2D (top) and 3D (bottom) representations of a fully cross-linked set of DETA and EPON 828 molecules

The priorities of primary and secondary amines in contribution to cross linking process can be different. There are two primary amines ($-NH_2$) and one secondary amine ($-NH-$) in DETA molecules. The activation energy of the primary reactions is less than that of secondary ones, especially in low temperatures [11]. However, in sufficiently high temperatures, as in this study, the difference in activation energies of primary and secondary reactions is negligible. With these considerations in mind, the second method with the same priority for the primary and secondary reactions was applied in this study.

Another important concern is final attainable degree of cross linking, i.e. the ratio of reacted sites to all possible reactive ones. It can be controlled through the cross linking cut-off distance, temperature, and to some extent, content of the curing agent. Cross linking cut-off distance is a crucial factor in obtaining desirable degrees of cross linking, and subsequently reasonable cross-linked structures. Taking small cut-off values will lead to small degrees of cross linking, and vice versa. In other words, the maximum attainable conversion will be restricted by the cut-off value, as the creation of covalent bonds can occur solely within a predefined cut-off distance around the reaction sites. Therefore, in order to achieve high degrees of cross linking, large or even no cut-off values must be imposed. In such cases, on the other hand, the resulted polymer will be excessively strained and difficult to get equilibrated. These issues should be taken into account for assigning appropriate cut-off distances.

The attraction force between pair of atoms beyond the large distances can be ignored. Different cut-off values, e.g. 4–10 Å [10, 15, 18–20], 5–10 Å [6], 7–8 Å [23] and 6 Å [32], have been applied in previous studies. Regardless of the attainable

degrees of cross linking, a cut-off value of 6 Å was adopted in our scheme to avoid highly strained structures.

Based on the given data, a 4-step cross linking procedure is proposed as follows:

Step 1. construction and energy minimization;

Based on the composition ratio of 5/2, an amorphous cell composed of 100 DGEBA and 40 DETA molecules (the weight fraction of 100:12 for DGEBA:DETA) with a low density of 0.5 g/cm^3 was constructed at room temperature and under periodic boundary conditions.

The system was subjected to energy minimization to reach the nearest local minimum. The minimization task employed both steepest descent and conjugate gradient (Fletcher-Reeves) algorithms, with the convergence criteria of 1000 kcal mol^{-1} and 10 kcal mol^{-1}, respectively.

Step 2. pre-equilibration;

Before starting the cross linking process, 500 ps isothermal-isobaric (NPT) dynamics with time step of 1 fs at 298 K and 1 atm was performed, to reach the real density and equilibrate the system. The Berendsen thermostat and barostat [52] were used to control, respectively, the temperature and pressure of the system during the equilibration. The time evolutions of the potential energy, temperature and density of the system were monitored during the dynamics, and the equilibrium state was confirmed as they got stable with slight fluctuations around constant values. The final density of blend reached the value of 1.08 g/cm^3.

Step 3. creation of covalent bonds;

As a cyclic combination of bonding-minimization-dynamics, step 3 was performed on the equilibrated structure. In each stage, the close contacts between pairs of reactive atoms were identified, and covalent bonds were created between the nearest pairs (within the cross linking cut-off distance). Thereafter, a minimization task, with the same criteria as in step 1, was performed, in order to release the stress imposed on the system. After minimization, the system was subjected to 300 ps high temperature canonical (NVT) dynamics at 500 K and 1 atm, in order to give enough kinetic energy to the molecules and increase the probability of curing sites to fall within the reaction cut-off distance. Again, the distances between the pairs of remaining reactive atoms were measured, and new covalent bonds were created, if possible. After each bond creation stage, the cross linking density (conversion rate) was calculated. The above stages were repeated until almost no new covalent bonds were possible to be created with the adopted cut-off distance (6 Å). During step 3, the cross linking density was controlled in each stage, and seven cross-linked structures beside the uncured system were stored individually in order to investigate the effect of cross linking density on the structure and properties of the epoxy polymers. Snapshots of the primary blend of reactants and final cross-linked structures with different conversion rates are represented in Fig. 4. The distribution and density of cross links in different structures is represented through the green-colored carbon atoms in epoxide groups of cross-linked chains.

Step 4. post-equilibration and sampling;

The final cross-linked samples were gradually cooled down to room temperature, at the rate of 20 K/100 ps, in the NVT ensemble, and then equilibrated through 500 ps NPT dynamics with the same settings as in step 2. Finally, 300 ps NVT dynamics was performed on the equilibrated systems, and generated configurations were stored every 1 ps, as the sampling trajectories for further analysis and calculation of the properties. The Nose-Hoover method [53, 54] was applied for controlling the temperature during sampling stage. The conversion rates and final densities of all structures are summarized in Table 1.

Calculation of the mechanical properties

There are three main approaches, static (constant − strain minimization) [57], dynamics (constant − stress molecular dynamics) [52, 58], and fluctuation formula [59–61], for calculation of the mechanical properties using MD simulations.

Fixed bond length and angle during deformation, and negligible effects of configurational entropy on the elastic constants are the main assumptions in static method [57, 62]. Nevertheless, reasonable results have been achieved using this method, making it more popular and frequently used than the dynamics and fluctuation methods. In contrast to static method, the dynamics approach brings the advantage of taking account of the entropic effects, and also making it possible to study the yielding of the material. However, it is a time consuming approach, and suffers from uncertainties in the results due to the strain fluctuations. The fluctuation method yields relatively reasonable results. However, slow convergence of elastic constants is the main drawback of the method, although it can be improved, to some extent, through the alternative fluctuation expression, developed by Gusev et al. [61].

The static method was used in current study to estimate the mechanical properties of the simulated systems. In the case of linear elastic materials, the stress–strain behavior can be described by generalized Hooke's law:

$$\sigma_{ij} = C_{ijkl}\varepsilon_{kl} \quad (1)$$

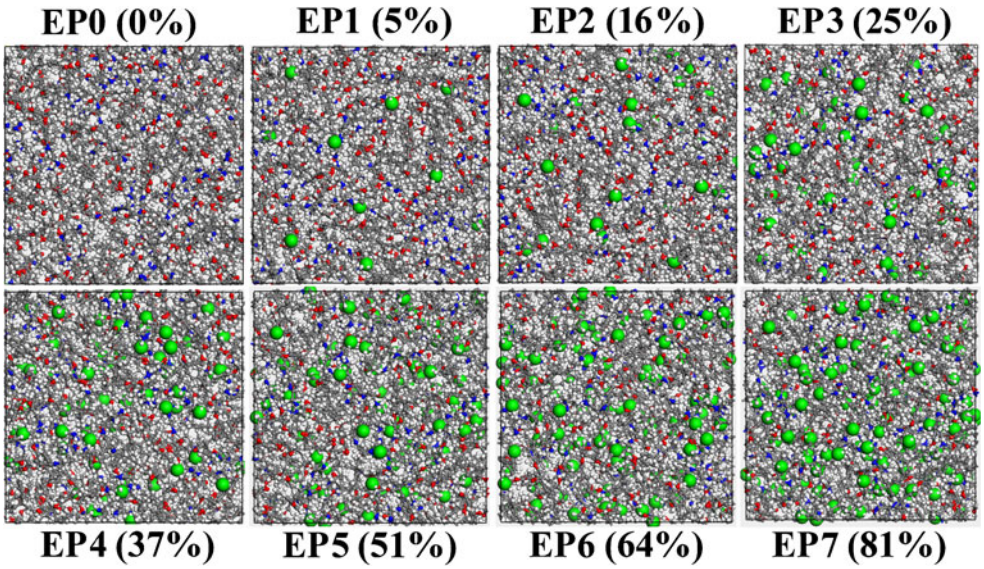

Fig. 4 Snapshots of the simulated polymer at different cross linking densities. The cross links are represented through the green-colored particles

where i, j, k, l=1, 2, 3. σ_{ij}, C_{ijkl} and ε_{kl} are stress, stiffness and strain tensors, respectively. The forth-order stiffness tensor has, in general, 81 components. The symmetry property of the stress and strain tensors ($\sigma_{ij} = \sigma_{ji}$ and $\varepsilon_{kl} = \varepsilon_{lk}$) leads to minor symmetries of the stiffness tensor, i.e. $C_{ijkl} = C_{jikl}$ and $C_{ijkl} = C_{ijlk}$, and consequently, results in reduction of independent components to 36. On the other hand, major symmetry of the stiffness tensor, resulted from strain energy [63], further reduces the number of independent components to 21. Therefore, Eq. (1) can be written in a second-order form, using Voigt notation:

$$\sigma_i = C_{ij}\varepsilon_j \tag{2}$$

where σ_i and ε_i are the 6-dimensional stress and strain vectors, and C_{ij} is the 6*6 stiffness matrix.

Calculation of the mechanical properties was initiated by pre-minimization of the structures, to make sure that the calculations are based on the most stable configurations. The pre-minimization was carried out using conjugate gradient algorithm with the convergence criteria of $2.0*10^{-5}$ kcal mol^{-1} for energy, 0.001 kcal mol^{-1} for force, and 10^{-5} Å for displacement. The minimized structures were strained under a set of 12 deformations (three pairs of uniaxial tension/compression and three pairs of pure shear), controlled by the corresponding strain vectors, with one component taking a tiny value, while the others kept fixed at zero, and then re-minimized without any change in cell parameters. The maximum strain amplitude was set to 0.001.

The elastic stiffness constants could then be obtained either using the energy approach, i.e. the second derivative of the deformation energy (U) per unit volume (V) with respect to strain:

$$C_{ij} = \frac{1}{V}\frac{\partial^2 U}{\partial\varepsilon_i \partial\varepsilon_j} \tag{3}$$

or alternatively through the virial theorem approach, i.e. the first derivative of the virial stress with respect to the strain, $\partial\sigma/\partial\varepsilon$, in which the stress components are obtained from the so-called virial expression:

$$\sigma_{ij} = -\frac{1}{V}\sum_k \left(m^k u_i^k u_j^k\right) + \frac{1}{2}\sum_{l\neq k}\left(r_i^{kl}\right) f_j^{lk}) \tag{4}$$

where V is the volume, m^k and u^k denote the mass and velocity of the kth particle, respectively, r^{kl} stands for the distance between kth and lth particles, and f^{lk} is the force exerted on lth particle by kth particle. In static conditions, as in our case, the stress tensor is given by Eq. (4) with the first term on the right hand side omitted.

The virial theorem approach was used in this study, due to its accuracy over the energy approach. In other words, the full 6*6 stiffness matrices were built up from the slopes $\partial\sigma/\partial\varepsilon$ in tension and shear. The Lamé

Table 1 Densities of the simulated structures with different conversion rates

Structure	Cross linking density (conversion rate)	Density (g/cm^3)	
		Simulation	Experiments
EP0	0 %	1.08	
EP1	5 %	1.10	
EP2	16 %	1.11	1.16 [38]
EP3	25 %	1.11	1.19 [55]
EP4	37 %	1.12	1.13 [56]
EP5	51 %	1.13	
EP6	64 %	1.14	
EP7	81 %	1.15	

coefficients, λ and μ, can be calculated using any two of the following equations:

$$\lambda = \frac{1}{6}(C_{12} + C_{13} + C_{21} + C_{23} + C_{31} + C_{32}) \approx \frac{1}{3}(C_{12} + C_{23} + C_{13}) \tag{5a}$$

$$\mu = \frac{1}{3}(C_{44} + C_{55} + C_{66}) \tag{5b}$$

$$\lambda + 2\mu = \frac{1}{3}(C_{11} + C_{22} + C_{33}) \tag{5c}$$

On the other hand, the stress–strain behavior of isotropic materials can be fully described using two independent Lamé coefficients:

$$\begin{pmatrix} \lambda+2\mu & \lambda & \lambda & 0 & 0 & 0 \\ \lambda & \lambda+2\mu & \lambda & 0 & 0 & 0 \\ \lambda & \lambda & \lambda+2\mu & 0 & 0 & 0 \\ 0 & 0 & 0 & \mu & 0 & 0 \\ 0 & 0 & 0 & 0 & \mu & 0 \\ 0 & 0 & 0 & 0 & 0 & \mu \end{pmatrix} \tag{6}$$

The particular combination of the zero and nonzero components in Eq. (6), and the symmetry of the matrix along the diagonal components are the main characteristics of an isotropic material. The other material properties can be simply calculated from the Lamé coefficients, as follows:

$$E = \frac{\mu(3\lambda + 2\mu)}{\lambda + \mu} \tag{7a}$$

$$K = \lambda + \frac{2}{3}\mu \tag{7b}$$

$$G = \mu \tag{7c}$$

$$\nu = \frac{\lambda}{2(\lambda + \mu)} \tag{7d}$$

where E, K and G stand for Young's, bulk and shear moduli, respectively, and ν denotes the Poisson's ratio.

Results and discussion

Mechanical properties

Presented here, are the 6*6 elastic stiffness matrices for uncured epoxy (EP0) and cross-linked EP7, calculated based on the procedure described in the previous section and averaged over the sampling trajectories:

$$C_{ij}^{EP0} = \begin{pmatrix} 4.11 & 1.67 & 1.65 & -0.02 & -0.08 & -0.04 \\ 1.67 & 4.09 & 1.83 & 0.00 & -0.06 & 0.03 \\ 1.65 & 1.83 & 4.23 & -0.02 & 0.04 & 0.02 \\ -0.02 & 0.00 & -0.02 & 1.01 & 0.04 & -0.02 \\ -0.08 & -0.06 & 0.04 & 0.04 & 1.10 & -0.04 \\ -0.04 & 0.03 & 0.02 & -0.02 & -0.04 & 1.02 \end{pmatrix} GPa$$

$$C_{ij}^{EP7} = \begin{pmatrix} 5.09 & 2.53 & 2.28 & -0.08 & -0.15 & 0.24 \\ 2.53 & 5.16 & 2.30 & 0.00 & -0.05 & 0.07 \\ 2.28 & 2.30 & 4.97 & -0.03 & 0.34 & -0.01 \\ -0.08 & 0.00 & -0.03 & 1.63 & 0.01 & 0.02 \\ -0.15 & -0.05 & 0.34 & 0.01 & 1.26 & -0.07 \\ 0.24 & 0.07 & -0.01 & 0.02 & -0.07 & 1.54 \end{pmatrix} GPa$$

Comparing the calculated stiffness matrices with Eq. (6), the isotropy condition of the simulated systems can be investigated. Although, those components of achieved matrices equivalent to zero components of Eq. (6) are not strictly zero, they are absolutely dominated by other components, and the deviations of the estimated elastic constants from the values suggested by Eq. (6) are negligible. Furthermore, the entire stiffness matrices are symmetrical with respect to their diagonal components. Therefore, the calculated elastic stiffness constants are reasonable and imply, with good approximation, the behavior of isotropic amorphous materials. The elastic stiffness constants of the other samples have similar characteristics. The averaged mechanical properties of all simulated structures, together with their standard deviations, are provided in Table 2, in comparison to some experimental values. As can be seen, there is good agreement between the simulations and experimental results, and increasing the cross linking density improves the mechanical properties of epoxy polymers.

As was pointed out earlier, the weight fraction of DGEBA:DETA and cross linking cut-off distance were considered 100:12 and 6 Å, respectively. It is evident that changing the content of hardener and cut-off value can influence the properties of yielded polymers, as they would change the attainable degrees of cross linking.

Local structures

Radial distribution function (RDF), also known as pair correlation function, g(r), can be defined as the probability of finding a given particle at a distance r from a reference

Table 2 Mechanical properties of the simulated systems (T = 300 K, DETA content = 12 pph) beside some experimental values (all moduli are in GPa)

Property	Simulation results								Experimental data
	EP0	EP1	EP2	EP3	EP4	EP5	EP6	EP7	
Elastic modulus (E)									3.4±0.1 [38]
									2.88±0.27 [39]
									3.57±0.08 [40]
	2.78	2.95	3.18	3.31	3.58	3.64	3.67	3.82	2.54±0.1 [43]
	(±0.18)	(±0.21)	(±0.23)	(±0.32)	(±0.13)	(±0.29)	(±0.31)	(±0.23)	2.6−3.9[a] [53]
									2.55±0.11 [54]
									3.86±0.06[b] [64][d]
									3.05±0.12[c] [64][d]
Bulk modulus (K)	2.75	2.79	2.84	2.86	2.92	3.06	3.09	3.11	–
	(±0.20)	(±0.24)	(±0.26)	(±0.23)	(±0.27)	(±0.28)	(±0.30)	(±0.26)	
Shear modulus (G)	1.04	1.11	1.21	1.26	1.38	1.40	1.41	1.48	–
	(±0.06)	(±0.10)	(±0.16)	(±0.12)	(±0.05)	(±0.10)	(±0.13)	(±0.08)	
Poisson's ratio(ν)	0.33	0.32	0.31	0.31	0.30	0.30	0.30	0.29	0.36±0.06 [64][d]
	(±0.02)	(±0.03)	(±0.02)	(±0.01)	(±0.03)	(±0.02)	(±0.02)	(±0.01)	

[a] the lowest and highest values at 298 K for DETA content of 12 pph

[b] nanoindentation test

[c] tension test

[d] the values are for DETA content 14 pph

particle. In order to study the local structures of the yielded polymers and investigate the influence of the cross linking density on the structure and properties of the epoxy polymers, RDFs of different pairs of atoms for equilibrated structures were calculated and averaged over the sampling trajectories at T = 300 K.

All-atom pair correlation functions of the EP0, EP1 and EP7 are plotted in Fig. 5. The RDF curves of all three models are similar, having a value of zero within short ranges due to excluded volume effect [7, 65], and smoothing at distances beyond 4–5 Å as a proof of lack of long-range order in the systems. Furthermore, at sufficiently far distances, inter-molecular RDFs approach unity, implying the behavior of amorphous materials in all cases. Generally, the peaks in the RDF curves within 3.5 Å are mainly due to hydrogen and chemical bonds between atoms, whilst those beyond 3.5 Å correspond to the van der Waals and electrostatic interactions [66, 67].

The peaks at distances around 0.9-1.1 Å are attributed to the direct chemical bonds between hydrogen and other atoms. The peaks at distances from 1.4 Å to 1.45 Å correspond to the direct C−N and C−O bonds, whilst those at around 1.75 Å come from the correlation between hydrogen atoms in the methyl ($-CH_3$) and methylene ($-CH_2-$) groups, and the subsequent intra-molecular peaks result from distances between atoms two bonds apart, such as hydrogen and carbon in H−C−C sequences (r=2.16 Å) and carbon atoms in C−C−C sequences (r=2.44 Å) [20]. The interactions between atoms separated by more than three bonds are represented by the farther minor peaks on intra-molecular RDFs.

For the uncured resin, EP0, and cross-linked EP1 and EP7, the inter-molecular interactions appear from 2 Å, and since $g_{total}(r) = g_{inter}(r) + g_{intra}(r)$, within the distance of 2 Å, $g_{total}(r)$ and $g_{intra}(r)$ are equal. The role of inter-molecular interactions becomes significant at farther separation distances. As can be seen in Fig. 5, with increasing the cross linking density, the intra-molecular RDFs approach zero in farther distances (7.5 Å for EP0 in comparison to 45 Å for EP7). This can be served as a measure of created cross links, and consequently the growth of polymer networks. The short chains of DGEBA and DETA in EP0 show short-range intra-molecular interactions, as is expected. In the case of cross-liked structures, however, it is revealed that longer chains are created, especially in the case of EP7.

There are four different atoms and more different atom types in the system, and since different atom types have individual roles in pair correlation functions, they were identified and labeled with their force field types using COMPASS notation, as is shown in Fig. 6a for DGEBA, DETA and cross-linked molecules. Some atom types are changed during the cross linking process. Breaking the C−O bonds in epoxide groups results in formation of hydroxyl (−OH) and methyl ($-CH_3$) groups, and changes the atom types of oxygen and carbon from *o2e* and *c4o* to *o2h* and *c4*, respectively. Creation of C−N bonds between DGEBA and DETA molecules changes the atom types of nitrogen in primary ($-NH_2$)

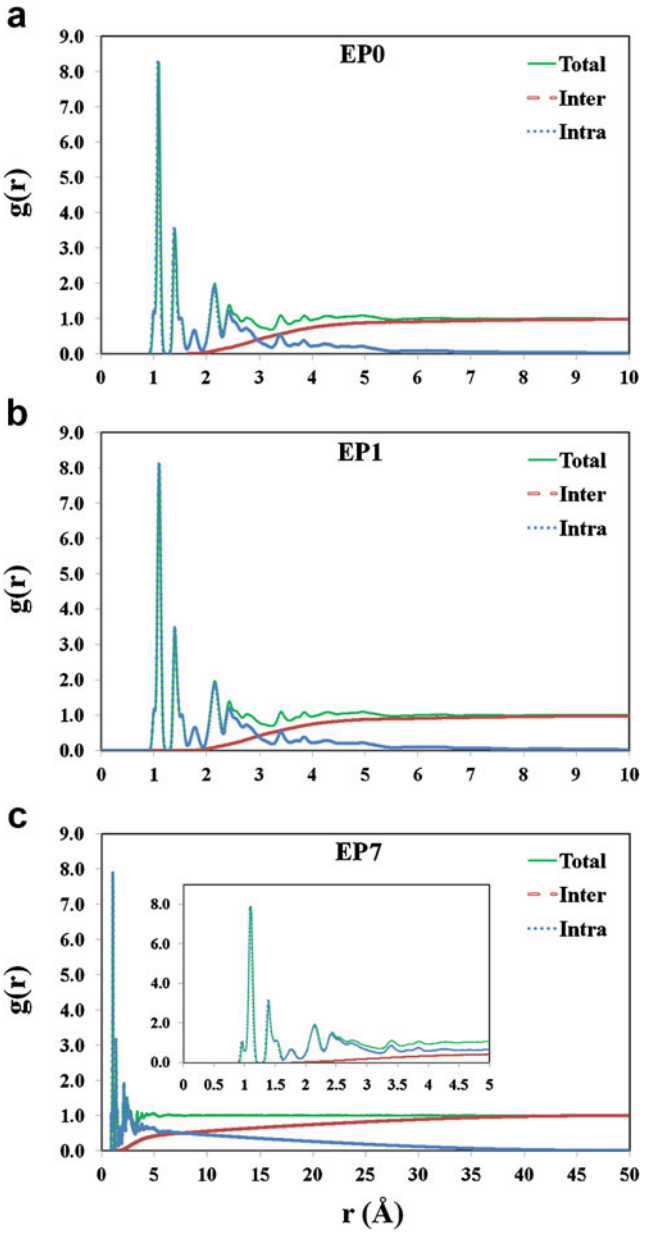

Fig. 5 Total, inter- and intra-molecular RDFs of all atoms for: **a** EP0, **b** EP1, and **c** EP7

and secondary (−NH−) amines from *n3h2* and *n3h1* to *n3h1* and *n3*, respectively.

Newly born *n3h1* atom types may be changed to *n3* atom types as the cross linking proceeds. As a consequence, increasing the cross linking density always decreases the number of *o2e*, c*4o* and *n3h2* atom types and increases the number of *o2h*, *c4* and *n3* ones. Successive birth and death of the *n3h1* atom type results in the growing trend of this atom type for the cross linking densities up to 37 %, and then decreasing trend for conversion rates of 51 %, 64 % and 81 % (Fig. 6b). In other words, the conversion of *n3h2* to *n3h1* for cross linking densities up to 37 %, and the conversion of *n3h1* to *n3* for higher cross linking densities are the dominant events.

Figure 7 shows the inter- and intra-molecular RDFs of N−O correlation. Three sharp peaks appear in intra-molecular RDFs at around 3 Å, 3.8 Å and 4.3 Å (Fig. 7a). Before cross linking, the nitrogen and oxygen atoms can be found solely in DETA and DGEBA molecules, respectively. Therefore, in the case of EP0, there is no intra-molecular relationship between N and O atoms in whole separation distances. After cross linking as a result of bond creation between C atoms of DGEBA and N atoms of DETA, there would be no direct bond between O and N atoms. Hence, for cross-linked structures (EP1 to EP7), the intra-molecular N−O RDF peaks appear in far distances. Actually, the appeared peaks are mainly due to correlations between N and O atoms three or four bonds apart, such as in O−C−C−N and O−C−C−C−N sequences. Furthermore, all peaks are enhanced with increasing the cross linking density. Both *o2h* and *o2e* atom types, depending on the spatial orientation of the DGEBA and connected DETA molecules, contribute in appeared peaks.

The inter-molecular correlations between N and O atoms are plotted in Fig. 7b. The first peaks at around 3.1 Å correspond to hydrogen bonds between polar atoms in distinct chains, and the second peaks at around 4.9 Å correspond to non-bonded inter-chain interactions, i.e. van der Waals and electrostatic. Inter-molecular RDFs decrease with increasing the cross linking density, indicating that the cross linking reduces the inter-chain interactions, as is expected.

The RDFs of the C−C, C−N and C−O pairs were also calculated for distances up to 20 Å. Similar to N−O pair, the inter-molecular RDFs of these pairs decrease with increasing the conversion rate as a consequence of reduced non-bonded interactions between the individual chains.

The intra-molecular RDFs of C−C, C−N and C−O pairs are plotted in Fig. 8a–c. In all three cases, no considerable intra-molecular correlation was found at distances farther than 5 Å, and hence RDFs are plotted in Fig. 8a–c for separation distances up to 5 Å. The first sharp peak at around 1.4 Å in Fig. 8a corresponds to partial double bonds between carbon atoms in the benzene rings of DGEBA and also C−C bonds in unreacted epoxide groups of DGEBA. The second peak at around 1.55 Å covers the remaining direct C−C bonds in either DGEBA or DETA molecules. The subsequent intra-molecular peaks are attributed to correlations of the carbon atoms two or more bonds apart, such as those in C−C−C and C−N−C (2.4 Å to 2.6 Å), C−C−C and C−C−O−C (2.8 Å), C−N−C−C (3.8 Å), and C−C−C−O−C (4.3 Å) sequences. Another noticeable point in Fig. 8a is the dependence of the RDFs on the cross linking density. The height of all peaks increase with increasing the cross linking density, except for those at around 1.4 Å and 2.8 Å. As the cross linking does not affect the bond length in benzene rings, the change in height of the peaks at around 1.4 Å comes from the variation of C−C bond length in epoxide groups. Before the reaction, the C−C bond

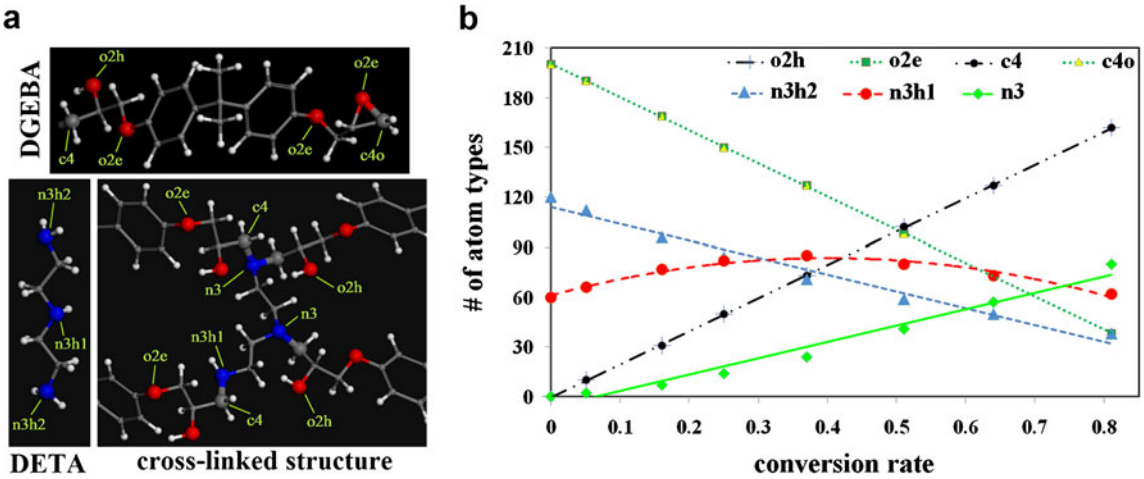

Fig. 6 **a** Representative DGEBA, DETA and cross-linked chains with typical atom types, labeled with COMPASS notation. **b** variation in the number of different atom types with respect to the cross linking density

length in epoxide group is about 1.4 Å, while the length of the same bond increases to 1.6 Å, upon cross linking. In other words, as cross linking proceeds, the contribution of C−C bonds of epoxide groups to RDF plots shifts from the first peak to the second one. This is why the first peaks decrease and the second ones increase in magnitude with increasing the cross linking density. Similarly, difference in some bond lengths and spatial orientation of chains before and after cross linking cause the forth peaks show opposite trend with increasing the cross linking density.

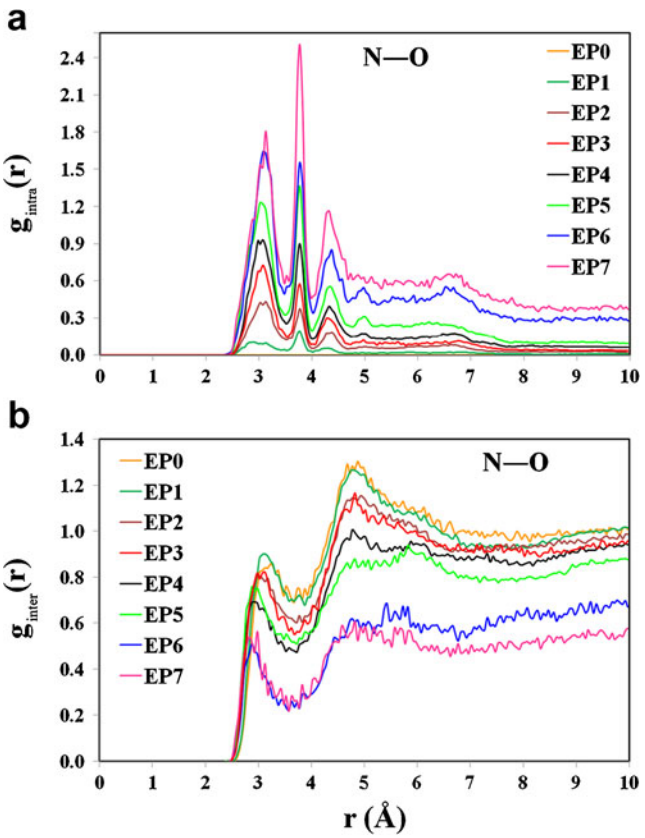

Fig. 7 **a** Intra- and **b** inter-molecular N−O pair correlation functions, at different cross linking densities

The intra-molecular RDFs of C−N correlation are plotted in Fig. 8b. Two major peaks are observed in $g_{intra}(r)$. The first one at around 1.45 Å belongs to direct C−N bonds and enhanced with increasing the conversion rate, proving the creation of new C−N bonds upon cross linking. The second one at around 2.55 Å attributes to correlations between atoms two bonds apart in C−C−N sequences either in DETA molecules (*c4*−*c4*−N) or between connected DGEBA and DETA molecules (*c43o*−*c4*−N), where N can be one of the *n3h2*, *n3h1* and *n3* atom types. By addition of the cross links, the correlation between non-adjacent C and N atoms increases and consequently enhances the magnitude of second RDF peaks, as is shown in Fig. 8b.

Represented in Fig. 8c, are the intra-molecular RDFs of C−O pair. The first peak at around 1.4 Å comes from direct C−O bonds and decreases with increasing the conversion rate, because of breaking the C−O bonds in epoxide groups upon activation (Fig. 2). The second peak at around 2.45 Å attributes to correlations between atoms two bonds apart in C−C−O sequences in DETA molecules. The magnitude of the second peak increases with increasing the cross linking density, due to conversion of the C−O direct bonds in primary epoxide groups to the C−C−O sequences in activated and reacted ones. In other words, the interaction between the C and O atoms in the epoxide groups (direct or two bonds apart) affects the magnitude of the first and second RDF peaks in a contrary manner. The last minor peaks are because of correlation between C and O atoms four bonds apart in C−N−C−C−O or C−O−C−C−O sequences, and

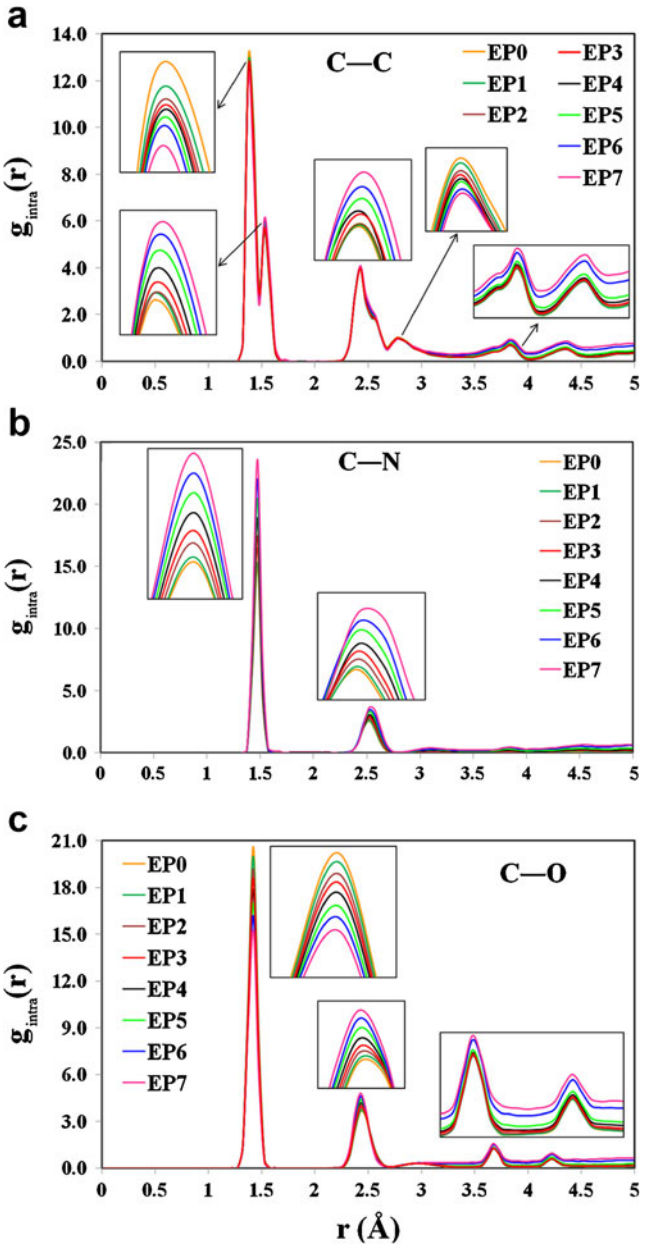

Fig. 8 Intra- molecular correlation functions of: **a** C−C, **b** C−N, and **c** C−O pairs, at different cross linking densities

are enhanced with increasing the conversion rate because of the activation of epoxide groups and connection of DETA molecules, both of which increase the number of above sequences.

Intra-molecular correlations of C−H, N−H and O−H were also considered in this study. Investigation of intra-molecular hydrogen bonding between polar atoms is possible using the plotted RDFs (Fig. 9). As is illustrated in Fig. 9a, two major and some minor peaks appear in $g_{intra}(r)$ of C−H correlation. The first peak at around 1.1 Å is attributed to direct covalent bonds between carbon and hydrogen atoms, and decreases with increasing the conversion rate because the number of hydrogen atoms covalently bonded to carbon atoms decreases upon cross-linking. Since the number of carbon atoms contributing in the cross linking process is very small in comparison to the whole, the variation in the magnitude of first peaks with respect to the cross linking density is not noticeable. The second peak in Fig. 9a, ranging from 2 Å to 2.35 Å, attributes to correlations two bonds apart in C−C−H and C−N−H sequences, and again decreases with conversion rate, due to formation of cross links and reduction of hydrogen atoms bonded to carbons and nitrogens.

Figure 9b illustrates the intra-molecular pair correlation function of the N and H atoms. Again, the first peak at 1 Å

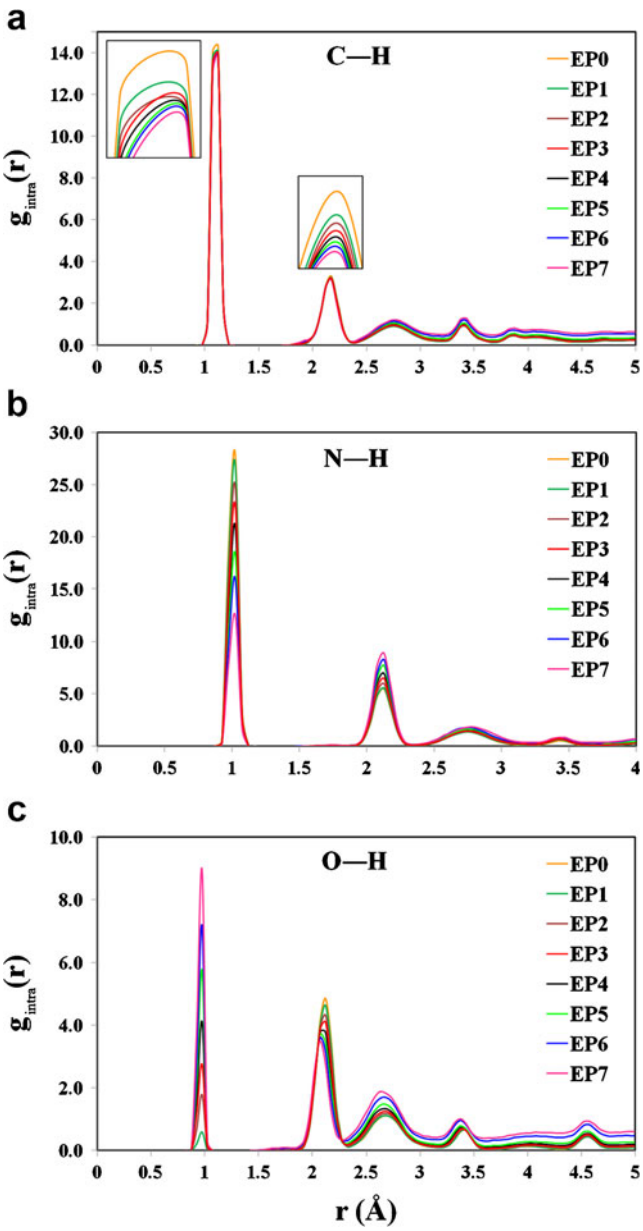

Fig. 9 Intra-molecular RDFs of: **a** C−H, **b** N−H, and **c** O−H pairs, at different cross linking densities

corresponds to the direct covalent bonds between the N and H atoms. Similar to the C−H correlation and for the same reason, the magnitude of the first peak decreases with increasing the cross linking density. However, because all nitrogen atoms can contribute in cross linking process, the variation in the peak height with respect to the conversion rate is considerable. The second peak in Fig. 9b, ranging from 2 Å to 2.3 Å, corresponds to the correlations two bonds apart in N−C−H sequences, either in DETA molecules or between connected DGEBA and DETA molecules, and increases with conversion rate due to formation of cross links and creation of new N−C−H sequences. The second peak can also be associated with the intra-molecular hydrogen bonding between the adjacent polar groups in the same chain (N as acceptor and C as donor), and increases directly as a function of conversion rate because the cross linking leads to connection of methylene ($-CH_2$) groups as new donors to acceptor N atoms. The subsequent broad minor peaks at around 2.75 Å and 3.4 Å correspond to correlations between N and H atoms three or four bonds apart in N−C−C−H, N−C−C−N−H atoms and N−C−C−O−H sequences. Theses peaks are enhanced with increasing the cross linking density due to formation of hydroxyl and methylene groups upon cross linking.

The intra-molecular RDFs of O−H pairs are represented in Fig. 9c. Direct covalent bonds between O and H atoms results in the first peak at around 0.95 Å. Owing to lack of any direct O−H bond in the primary structure of DGEBA, there is no peak for EP0 at 0.95 Å. For other structures, the appeared peaks are considerably enhanced with increasing the conversion rate, since the activation of epoxide groups leads to formation of new hydroxyl groups. The next peak at distances ranging from 2 Å to 2.3 Å corresponds to pair correlations between O and H atoms of the adjacent methylene bridges. Upon cross linking and due to changing the bond angles in epoxide groups, the distances between hydroxy oxygens and H atoms of the adjacent methylene groups increase and cause reduction in magnitude of the second peak. Moreover, the intra-molecular hydrogen bonds between the acceptor O atoms and donor C atoms contribute in formation of the second peak, and reduce its magnitude with increasing the conversion rate, because the cross linking leads to lack of adjacent donor C atoms in the same chain. The subsequent peaks, attributed to those atoms on the third or farther coordination circles of the oxygen (more than two bonds apart), are enhanced with increasing the cross linking density due to connection of new methylene and amine groups.

Conclusions

In this study, the molecular dynamics method with COMPASS force-field was successfully utilized to simulate the cross linking of DGEBA (epoxy EPON 828) with DETA curing agent, yielding polymer networks with different cross linking densities. The constant strain (static) approach was then adopted to calculate the mechanical properties of uncured and cross-linked structures. The simulation results revealed dependency of the mechanical properties on the cross linking density of the polymers. It was confirmed that increasing the cross linking density leads to improvements in the material properties. It can also be concluded that the material properties would be further enhanced by increasing the conversion rate through assigning larger reaction cut-off distances.

Comparing the simulation results with experimental data demonstrated the validity and accuracy of the presented cross linking scheme and modeled structures.

Finally, the radial distribution functions (RDFs) were used to study the local structures of the simulated polymers and investigate the structure evolution of the simulated systems with increasing the cross linking density. Moreover, RDFs revealed inverse relationship between the cross linking density and intensity of hydrogen bonds in the polymer networks.

References

1. Pascault J-P, Williams RJJ (2010) General Concepts about Epoxy Polymers. In: Pascault J-P, Williams RJJ (eds) Epoxy polymers. Wiley-VCH, Weinheim, pp 1–12. doi:10.1002/9783527628704ch1
2. Zeng QH, Yu AB, Lu GQ (2008) Multiscale modeling and simulation of polymer nanocomposites. Prog Polym Sci 33(2):191–269. doi:10.1016/j.progpolymsci.2007.09.002
3. Doherty DC, Holmes BN, Leung P, Ross RB (1998) Polymerization molecular dynamics simulations. I. Cross-linked atomistic models for poly (methacrylate) networks. Comput Theor Polym Sci 8(1–2):169–178
4. Tsige M, Stevens MJ (2004) Effect of cross-linker functionality on the adhesion of highly cross-linked polymer networks: a molecular dynamics study of epoxies. Macromol 37(2):630–637
5. Komarov PV, Yu-Tsung C, Shih-Ming C, Khalatur PG, Reineker P (2007) Highly cross-linked epoxy resins: an atomistic molecular dynamics simulation combined with a mapping/reverse mapping procedure. Macromol 40(22):8104–8113
6. Bermejo JS, Ugarte CM (2009) Chemical crosslinking of PVA and prediction of material properties by means of fully atomistic MD simulations. Macromol Theory Simul 18(4–5):259–267
7. Bermejo JS, Ugarte CM (2009) Influence of cross–linking density on the glass transition and structure of chemically cross–linked PVA: a molecular dynamics study. Macromol Theory Simul 18(6):317–327
8. Hölck O, Dermitzaki E, Wunderle B, Bauer J, Michel B (2011) Basic thermo-mechanical property estimation of a 3D-crosslinked epoxy/SiO2 interface using molecular modelling. Microelectron Reliab 51(6):1027–1034. doi:10.1016/j.microrel.2011.03.014
9. Tack JL, Ford DM (2008) Thermodynamic and mechanical properties of epoxy resin DGEBF crosslinked with DETDA by molecular dynamics. J Mol Graphics Modell 26(8):1269–1275
10. Varshney V, Patnaik SS, Roy AK, Farmer BL (2008) A molecular dynamics study of epoxy-based networks: cross-linking procedure and prediction of molecular and material properties. Macromol 41(18):6837–6842

11. Li C, Strachan A (2010) Molecular simulations of crosslinking process of thermosetting polymers. Polymer 51(25):6058–6070
12. Nouri N, Ziaei-Rad S (2011) A molecular dynamics investigation on mechanical properties of cross-linked polymer networks. Macromol 44(13):5481–5489. doi:10.1021/ma2005519
13. Bandyopadhyay A, Valavala PK, Clancy TC, Wise KE, Odegard GM (2011) Molecular modeling of crosslinked epoxy polymers: the effect of crosslink density on thermomechanical properties. Polymer 52(11):2445–2452. doi:10.1016/j.polymer.2011.03.052
14. Fan HB, Yuen MMF (2007) Material properties of the cross-linked epoxy resin compound predicted by molecular dynamics simulation. Polymer 48(7):2174–2178
15. Yu S, Yang S, Cho M (2009) Multi-scale modeling of cross-linked epoxy nanocomposites. Polymer 50(3):945–952
16. Choi J, Yu S, Yang S, Cho M (2011) The glass transition and thermoelastic behavior of epoxy-based nanocomposites: a molecular dynamics study. Polymer 52(22):5197–5203. doi:10.1016/j.polymer.2011.09.019
17. Yu S, Yang S, Cho M (2011) Multiscale modeling of cross-linked epoxy nanocomposites to characterize the effect of particle size on thermal conductivity. J Appl Phys 110(12):124302–124309
18. Wu C, Xu W (2006) Atomistic molecular modelling of crosslinked epoxy resin. Polymer 47(16):6004–6009
19. Wu C, Xu W (2007) Atomistic simulation study of absorbed water influence on structure and properties of crosslinked epoxy resin. Polymer 48(18):5440–5448
20. Wu C, Xu W (2007) Atomistic molecular simulations of structure and dynamics of crosslinked epoxy resin. Polymer 48(19):5802–5812
21. Hörstermann H, Hentschke R, Amkreutz M, Hoffmann M, Wirts-Rütters M (2010) Predicting water sorption and volume swelling in dense polymer systems via computer simulation. J Phys Chem B 114(51):17013–17024
22. Lin PH, Khare R (2009) Molecular simulation of cross-linked epoxy and epoxy − POSS nanocomposite. Macromol 42(12):4319–4327
23. Clancy T, Frankland S, Hinkley J, Gates T (2009) Molecular modeling for calculation of mechanical properties of epoxies with moisture ingress. Polymer 50(12):2736–2742
24. Prasad A, Grover T, Basu S (2010) Coarse–grained molecular dynamics simulation of cross–linking of DGEBA epoxy resin and estimation of the adhesive strength. Int J Eng Sci Technol 2(4):17–30
25. Liu H, Li M, Lu Z-Y, Zhang Z-G, Sun C-C, Cui T (2011) Multiscale simulation study on the curing reaction and the network structure in a typical epoxy system. Macromol 44(21):8650–8660. doi:10.1021/ma201390k
26. Chang S-H, Kim H-S (2011) Investigation of hygroscopic properties in electronic packages using molecular dynamics simulation. Polymer 52(15):3437–3442. doi:10.1016/j.polymer.2011.05.056
27. Soni NJ, Lin P-H, Khare R (2012) Effect of cross-linker length on the thermal and volumetric properties of cross-linked epoxy networks: a molecular simulation study. Polymer 53(4):1015–1019. doi:10.1016/j.polymer.2011.12.051
28. Gou J, Minaie B, Wang B, Liang Z, Zhang C (2004) Computational and experimental study of interfacial bonding of single-walled nanotube reinforced composites. Comput Mater Sci 31(3):225–236
29. Zhu R, Pan E, Roy A (2007) Molecular dynamics study of the stress–strain behavior of carbon-nanotube reinforced Epon 862 composites. Mater Sci Eng, A 447(1):51–57
30. Ionita M (2012) Multiscale molecular modeling of SWCNTs/epoxy resin composites mechanical behaviour. Compos Part B: Eng 43(8):3491–3496. doi:10.1016/j.compositesb.2011.12.008
31. Deazle A, Hamerton I, Heald C, Howlin B (1996) Molecular modelling of high performance polymers. Polym Int 41(2):151–157
32. Yarovsky I, Evans E (2002) Computer simulation of structure and properties of crosslinked polymers: application to epoxy resins. Polymer 43(3):963–969
33. Wunderle B, Dermitzaki E, Hölck O, Bauer J, Walter H, Shaik Q, Rätzke K, Faupel F, Michel B, Reichl H (2010) Molecular dynamics approach to structure–property correlation in epoxy resins for thermo-mechanical lifetime modeling. Microelectron Reliab 50(7):900–909
34. Abbott LJ, Colina CM (2011) Atomistic structure generation and gas adsorption simulations of microporous polymer networks. Macromol 44(11):4511–4519. doi:10.1021/ma200303p
35. Li Y, Kröger M, Liu WK (2011) Primitive chain network study on uncrosslinked and crosslinked cis-polyisoprene polymers. Polymer 52(25):5867–5878. doi:10.1016/j.polymer.2011.10.044
36. Song X, Sun Y, Wu X, Zeng F (2011) Molecular dynamics simulation of a novel kind of polymer composite incorporated with polyhedral oligomeric silsesquioxane (POSS). Comput Mater Sci 50(12):3282–3289. doi:10.1016/j.commatsci.2011.06.009
37. Kessler M, Sottos N, White S (2003) Self-healing structural composite materials. Compos Part A: Appl Sci Manuf 34(8):743–753
38. Brown E, White S, Sottos N (2006) Fatigue crack propagation in microcapsule-toughened epoxy. J Mater Sci 41(19):6266–6273
39. Blaiszik B, Sottos N, White S (2008) Nanocapsules for self-healing materials. Compos Sci Technol 68(3):978–986
40. Yuan YC, Rong MZ, Zhang MQ, Chen J, Yang GC, Li XM (2008) Self-healing polymeric materials using epoxy/mercaptan as the healant. Macromol 41(14):5197–5202
41. Liu X, Sheng X, Lee JK, Kessler MR, Kim JS (2009) Rheokinetic evaluation of self-healing agents polymerized by Grubbs catalyst embedded in various thermosetting systems. Compos Sci Technol 69(13):2102–2107
42. Jin H, Mangun CL, Stradley DS, Moore JS, Sottos NR, White SR (2012) Self-healing thermoset using encapsulated epoxy-amine healing chemistry. Polymer 53(2):581–587. doi:10.1016/j.polymer.2011.12.005
43. Neuser S, Michaud V, White SR (2012) Improving solvent-based self-healing materials through shape memory alloys. Polymer 53(2):370–378. doi:10.1016/j.polymer.2011.12.020
44. http://accelrys.com/products/materials-studio/ Accelrys Inc., San Diego.
45. Sun H (1998) COMPASS: An ab initio force-field optimized for condensed-phase applications overview with details on alkane and benzene compounds. J Phys Chem B 102(38):7338–7364
46. Fried J (1998) The COMPASS force field: parameterization and validation for phosphazenes. Comput Theor Polym Sci 8(1–2):229–246
47. Bunte SW, Sun H (2000) Molecular modeling of energetic materials: the parameterization and validation of nitrate esters in the COMPASS force field. J Phys Chem B 104(11):2477–2489
48. Yang J, Ren Y, Tian A, Sun H (2000) COMPASS force field for 14 inorganic molecules, He, Ne, Ar, Kr, Xe, H2, O2, N2, NO, CO, CO2, NO2, CS2, and SO2, in liquid phases. J Phys Chem B 104(20):4951–4957
49. McQuaid MJ, Sun H, Rigby D (2004) Development and validation of COMPASS force field parameters for molecules with aliphatic azide chains. J Comput Chem 25(1):61–71
50. Rigby D (2004) Fluid density predictions using the COMPASS force field. Fluid Phase Equilib 217(1):77–87
51. Ewald PP (1921) Die Berechnung optischer und elektrostatischer Gitterpotentiale. Ann Phys 369(3):253–287
52. Berendsen HJC, Postma JPM, Van Gunsteren WF, DiNola A, Haak J (1984) Molecular dynamics with coupling to an external bath. J Chem Phys 81:3684
53. Nosé S (1984) A molecular dynamics method for simulations in the canonical ensemble. Mol Phys 52(2):255–268. doi:10.1080/00268978400101201
54. Hoover WG (1985) Canonical dynamics: equilibrium phase-space distributions. Phys Rev A 31(3):1695–1697
55. Shell Chemical Co (1989). EPON resin structural reference manual. Shell Chemical Co, Houston
56. Garcia FG, Soares BG, Pita VJ, Sánchez R, Rieumont J (2007) Mechanical properties of epoxy networks based on DGEBA and aliphatic amines. J Appl Polym Sci 106(3):2047–2055

57. Theodorou DN, Suter UW (1986) Atomistic modeling of mechanical properties of polymeric glasses. Macromol 19(1):139–154
58. Brown D, Clarke JHR (1991) Molecular dynamics simulation of an amorphous polymer under tension. 1. Phenomenology. Macromolecules 24(8):2075–2082
59. Parrinello M, Rahman A (1982) Strain fluctuations and elastic constants. J Chem Phys 76:2662
60. Ray JR (1988) Elastic constants and statistical ensembles in molecular dynamics. Comput Phys Rep 8(3):109–151. doi:10.1016/0167-7977(88)90009-3
61. Gusev AA, Zehnder MM, Suter UW (1996) Fluctuation formula for elastic constants. Phys Rev B 54:1–4
62. Raaska T, Niemela S, Sundholm F (1994) Atom-based modeling of elastic constants in amorphous polystyrene. Macromolecules 27(20):5751–5757
63. Sadd MH (2009) Elasticity: theory, applications, and numerics. Academic Press, Burlington
64. Possart G, Presser M, Passlack S, Geifl P, Kopnarski M, Brodyanski A, Steinmann P (2009) Micro–macro characterisation of DGEBA-based epoxies as a preliminary to polymer interphase modelling. Int J Adhes Adhes 29(5):478–487
65. Yang S, Qu J (2012) Computing thermomechanical properties of crosslinked epoxy by molecular dynamic simulations. Polymer 53(21):4806–4817
66. Liu J, Liu Z, Yuan S, Liu J (2013) Synthesis, crystal structures, and spectral characterization of tetranuclear Mn(II) complex with a new Schiff base ligand and molecular dynamics studies on inhibition properties of such Schiff base. J Mol Struct 1037:191–199
67. Zeng JP, Zhang JY, Gong XD (2011) Molecular dynamics simulation of interaction between benzotriazoles and cuprous oxide crystal. Comput Theor Chem 963:110–114